Materials Science Research International, Vol.7, No.1 pp.27-33 (2001)

General paper

Simulation of the Forging Process Incorporating Strain-Induced Phase Transformation Using the Finite Volume Method (Part II; Effects of Strain Rate on Structural Change and Mechanical Behavior)

Peiran DING*, Dong-Ying JU**, Tatsuo INOUE***, Shoji IMATANI*** and Edwin de VRIES ****

*Technical Division, MSC.Software Japan Ltd., 2-39, Akasaka 5-Chome, Minato-ku, Tokyo, Japan

**Department of Mechanical Engineering, Saitama Institute of Technology, Fusaiji 1690, Okabe, Saitama, Japan

***Department of Energy Conversion Science, Kyoto University, Sakyo-ku, Kyoto, Japan

****MSC.Software (E.D.C.) B.V., Groningenweg 6, 2803 PV, Gouda, The Netherlands

Abstract: In Part I, based on the framework of *metallo-thermo-mechanics*, a finite volume method formulated in the Eulerian description has been set up to simulate the forging process and corresponding strain-induced austenitic-martensite phase transformation. The approach has been developed and implemented in the commercial computer program MSC.SuperForge. In this paper, numerical simulations for SUS304 stainless steel on backward and forward extrusions are carried out in order to verify the method proposed in Part I. Furthermore, the effects of strain rate on the austenitic-martensite phase transformation and the aggregate flow stress are studied.

Key words: *Finite volume method, Strain-induced phase transformation, Incremental formulation of kinetics equation, Metallo-thermo-mechanics, Forging, SUS304 stainless steel, Strain rate*

1. INTRODUCTION

In Part I of this series of papers, a description of the *finite volume method* is presented as it relates to simulating metallic structure, temperature and stress/strain in the forging process associated with *strain-induced phase transformation* based on the *metallo-thermo-mechanics* [1,2]. The deforming workpiece flows through fixed finite volume meshes using the Eulerian formulation to describe the conservation laws. This is particularly suited for large three-dimensional material deformation such as forging since remeshing techniques are not required.

The austenitic stainless steel SUS304 is chosen for the study because of its obvious practical importance and notable micro-structural phenomena that occur during the forging process. It is well known that an austenitic-martensite phase transformation takes place according to the strain and temperature during plastic deformation [3-14]. This phase transformation is called *strain-induced austenitic-martensite phase transformation*. It can be developed at low temperature and almost completely inhibited at higher temperature within usual strain ranges. In this research, the incremental expression on the formulation of the kinetics equation is derived by use of Tsuta and Cortes' model [10].

Mechanical deformation in the forging process is usually so large that the heat generated by the dissipation of plastic work is not negligible. Due to this deformation and heat conduction, a temperature gradient develops in the workpiece. The variation in strain and temperature in the workpiece will affect the amount of martensite transformation.

The aggregate flow stress of the austenite and martensite constituents is affected by the respective flow stresses and phase transformation. We call macroscopic stress in the conventional meaning as *aggregate stress* in order to emphasize that this stress acts on the whole mixture, while *respective flow stress* is also used when the term designates distinctive stress acting on each constituent. As a result of martensite phase transformation, the hardening increases rapidly with the deformation of the material during the forging process. We consider the structure evolution in order to understand ultimately the complete flow stress and other mechanical behavior.

More attention should be paid to the effects of strain rate on structural change and mechanical behavior. Early experimental work by Powell [3] at high strain rates ($\sim 10^3$ s^{-1}) shows that the amount of martensite decreases with increasing strain rate. Powell concluded that the increased stability of the austenite resulted from adiabatic heating at high strain rates. Hecker et al. [6,7] made a series of uniaxial and biaxial tests under different strain rates and came up with the same conclusion. It is obvious that the influence of the strain rate is quite important. Nevertheless, the numerical analysis of the effects of strain rate on structural change and mechanical behavior is still lacking. Most of the simulations are limited to the low strain rate range ($\sim 10^{-3}$ s^{-1}) except for the simulation by Tomita et al. [8], in which a process of tension test for sheet specimen of SUS304 steel was simulated by the finite element method when taking strain rate dependency into account.

In this paper, simulations of temperature, structural evolution and stress/strain in the course of backward and forward extrusions are carried out by applying the method described in Part I. In order to verify the validity of the simulated results, comparisons are made with the experimental data by Tsuta and Cortes [14]. The strain rate dependence of the flow stress is formulated. The effects of strain rate on the austenitic-martensite transformation and the aggregate flow stress are studied.

Received September 12, 2000
Accepted February 6, 2001

Table 1. Chemical composition of SUS304 used (wt%).

C	Si	Mn	P	S	Ni	Cr	Cu	Mo	N
0.034	0.36	1.07	0.026	0.008	9.88	18.17	0.12	0.15	0.035

2. NUMERICAL MODELS

Simulations on backward and forward extrusions are carried out. The experimental results are provided by Tsuta [14]. The material used in the experiments was SUS304 austenitic stainless steel, whose chemical composition is shown in Table 1. Specimens were machined into cylindrical billets of 14.0 mm in diameter and 10.5 mm in height.

In order to verify the three-dimensional ability of the program, the numerical models are generated in three dimensions shown in Fig. 1. Because of the axi-symmetric condition, triangular prismatic meshes are used with head angles of 30 deg. All the dies are modeled as rigid bodies. The initial temperature of the billets and dies is 15 °C, while the steady temperature of the environment is taken as 15 °C.

Investigations in [9,15-17] have shown that the strain hardening for SUS304 stainless steel in austenite state exhibits flow curves that can be described as:

$$\bar{\sigma}_A = K(\bar{\varepsilon}^p)^n . \quad (1)$$

Here, $\bar{\varepsilon}^p$ is the equivalent plastic strain. In order to consider material hardening due to strain rate, the flow constant K depends on the equivalent strain rate $\dot{\bar{\varepsilon}}$ as:

$$K = K_0\left(\dot{\bar{\varepsilon}}/\dot{\bar{\varepsilon}}_0\right)^m , \quad (2)$$

where $\dot{\bar{\varepsilon}}_0$ is the reference strain rate equal to $5.0\text{x}10^{-4}$ s^{-1} and m is the strain rate sensitivity equal to 0.013 [8]. The material parameters K_0, n in the above equations are experimentally determined to be 560.0 MPa, 0.18, respectively.

On the other hand, the flow stress contribution of martensite may be defined as follows according to Ludwigson et al. [9]:

$$\bar{\sigma}_M = C(\xi_M)^Q . \quad (3)$$

Here, the material parameters C, Q in the above equations are experimentally determined to be 1260.0 MPa and 1.27, respectively.

The volumetric dilatation due to structural change, the latent heat generated in the course of austenite-martensite phase transformation and the intensity of austenite-martensite phase transformation plasticity (see Eq.(15) in Part I) are taken as $7.3\text{x}10^{-4}$, $1.5\text{x}10^4$ J/kg and $5.08\text{x}10^{-5}$ MPa^{-1} [1,8,18], respectively.

The heat transfer plays a very important role here because adiabatic heating can inhibit the transformation and thereby influence the plastic flow. The heat transfer coefficient between workpiece and die is taken as $1.74\text{x}10^4$ W/(m^2·K) while that between workpiece/die and ambient is 10.4 W/(m^2·K) according to Ref. [14].

Other properties such as the coefficient of heat conduction, specific heat and elastic modulus, which are dependent upon the content of each phase and temperature, are taken to be the same as Part I. The thermal expansion coefficient is constant as $1.5\text{x}10^{-5}$ 1/K for austenite and $1.1\text{x}10^{-5}$ 1/K for martensite.

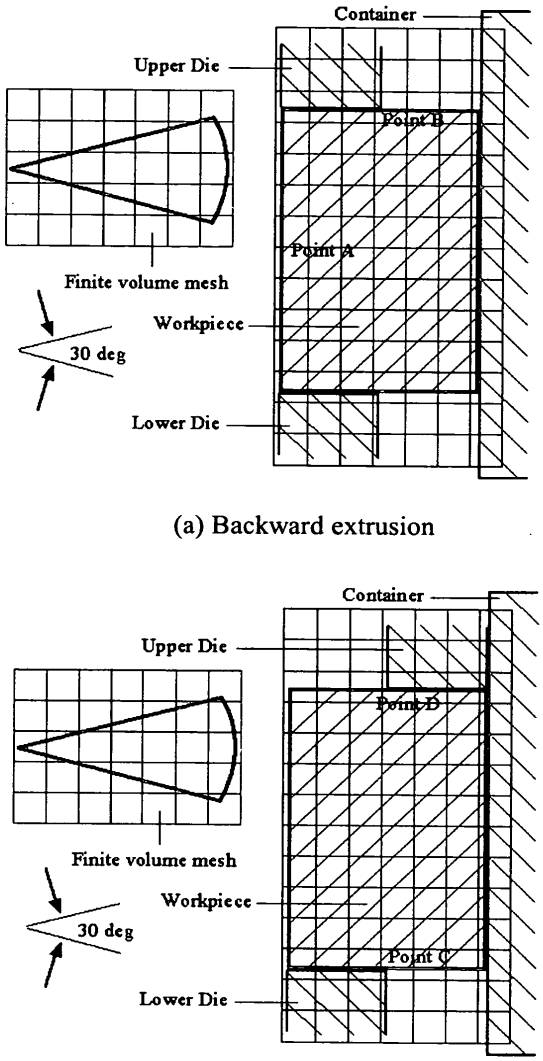

(a) Backward extrusion

(b) Forward extrusion

Fig. 1. Schematic illustration of numerical models.

3. SIMULATED RESULTS AND DISCUSSION

In order to study the effect of strain rate on the austenitic-martensite phase transformation and the aggregate flow stress, the simulations are carried out with a series of constant extruding speeds from 0.0015 mm/s to 1.5 m/s on the upper dies with respect to the fixed lower dies as shown in Table 2. The speed induces the lowest strain rate ($\sim 10^{-3}$ s^{-1}) and the highest one ($\sim 10^{3}$ s^{-1}). The stroke is 4.8mm for backward extrusion and 3.4mm for forward extrusion, respectively.

3.1. Validity with Experimental Data

Figure 2 shows the deformation modes of the billets for some representative strokes.

Table 2. Cases of simulation.

Die speed (m/s)	1.5×10^{-6} (slow)	1.5×10^{-4}	1.5×10^{-2}	1.5 (fast)
Strain rate	10^{-3} (low)	10^{-1}	10	10^{3} (high)

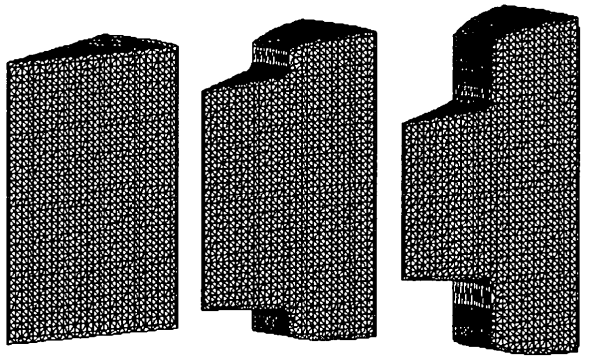

0 mm (initial) 2.4 mm (middle) 4.8 mm (final)

(a) Backward extrusion

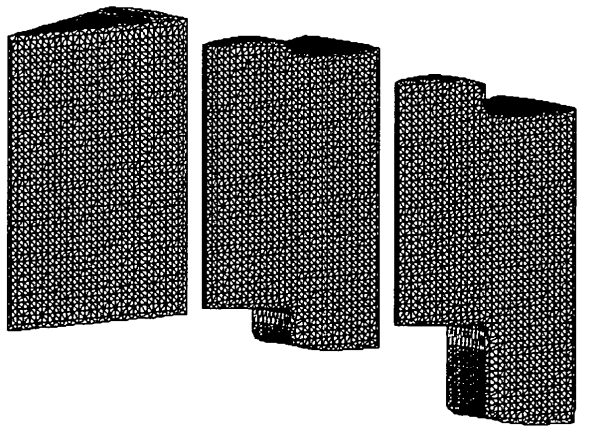

0 mm (initial) 1.7 mm (middle) 3.4 mm (final)

(b) Forward extrusion

Fig. 2. Deformation modes of the billets.

The variation of the shape is successfully encapsulated by a geometric surface comprised of triangular facets. The Resolution Enhancement Technology (RET) algorithm is employed to automatically refine the facet surface through the simulation to capture the continuous change and the increasing complexity of the deforming material.

Comparisons between measured and simulated martensite distributions (low strain rate only corresponding to the experiment) at the end of the process for each model are shown in Figs. 3 and 4. The volume fraction of martensite was measured by the magnetic balance method in the experiment. The simulation successfully duplicates the martensite transformation, and the results show a good agreement in tendency with the experimental data.

As shown in Fig. 3, the simulation of backward extrusion gives slight unsymmetric results for the upper part and the lower part separated by the middle horizontal plane since the upper die moves but the lower die remains stationary. This tendency can be also observed in the experimental data.

Figure 5 depicts the simulated forging load (low strain rate only corresponding to the experiment) with the experimentally determined load. It is observed that a good agreement between simulated and experimental results is obtained in both cases of backward and forward extrusion.

3.2. Effects of Strain Rate on Temperature and Volume Fraction of Martensite

The simulated results of temperature and volume fraction of martensite are depicted in Figs. 6 (a) and (b) for the backward extrusion model at points A and B during the forging stage. As shown in Fig. 1(a), point A is in the center of billet while point B is on the surface of the billet at the corner of the upper die. The results of simulation for the forward extrusion are shown in Fig. 7. Here, point C is on the surface of billet at the corner of the lower die and point D is on the surface of billet at the corner of the upper die as shown in Fig. 1(b).

Attention should be paid to the influence of strain rate on phase transformation of the SUS304 steel. The plastic strain with respect to the change of strain rate displays minor differences as long as the stroke is the same. But the temperature rises more readily in high strain rate than in low strain rate during the deformation. The martensite formation is found to be considerably less in high strain rate. The temperature increase resulting from the heat generated by the dissipation of plastic work is sufficient to suppress the austenitic-martensite phase transformation. These phenomena can also be observed clearly in Figs. 8 and 9, in which temperature and volume fraction of martensite are depicted versus the strain rate for both cases of the backward and forward extrusion at the end of the processes.

3.3. Evolution of Flow Stress

The simulated equivalent stresses at points A and B for the backward extrusion and at points C and D for the forward extrusion with progressive stroke are depicted in Figs. 10 and 11, respectively. These figures show that the aggregate flow stress of the austenite and martensite

constituents is affected by the respective flow stresses and phase transformation. At low strain levels, the hardening behavior of the material is determined mainly by austenite. According to Eqs. (1) and (2), the higher strain rate causes stronger austenite hardening. The stresses in high strain rate are higher than the stresses in low strain rate during the beginning of the stroke. However, with the generation of martensite, the flow stress becomes highly dependent on the martensite content of the material. The low strain rate gives much higher stresses at the end of simulations due to the larger amount of martensite.

The simulated equivalent stress distributions in both low and high strain rates at the end of the process are plotted in Figs. 12 and 13. It is obvious that the stress distributions in both strain rates have a similar pattern as the martensite distributions. The status of stress at the end of the process is determined by the martensite content. The stress in high strain rate is much lower than that in low strain rate because the martensite formation is less in high strain rate. It shows that the structure evolution is very pre-requisite for understanding the complete flow stress and other mechanical behavior.

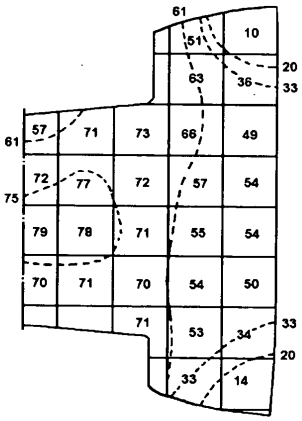

(a) Measured [14]

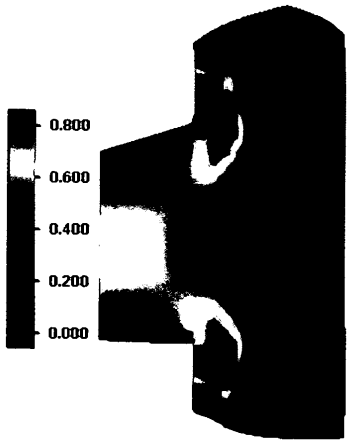

(b) Calculated

Fig. 3. Experimental measured and calculated martensite distributions after backward extrusion.

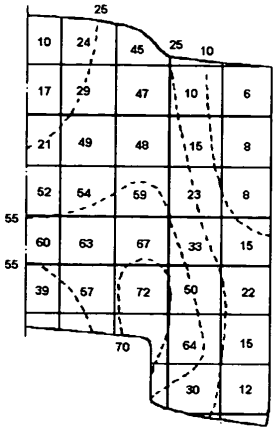

(a) Measured [14]

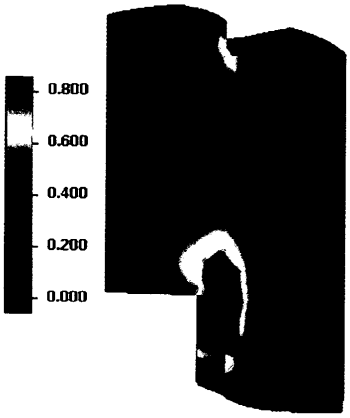

(b) Calculated

Fig. 4. Experimental measured and calculated martensite distributions after forward extrusion.

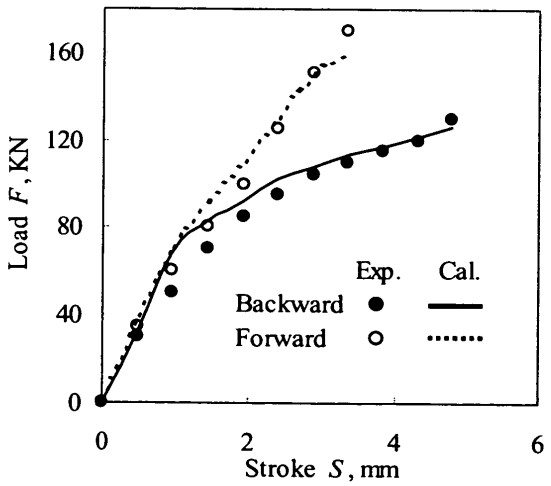

Fig. 5. Forging load.

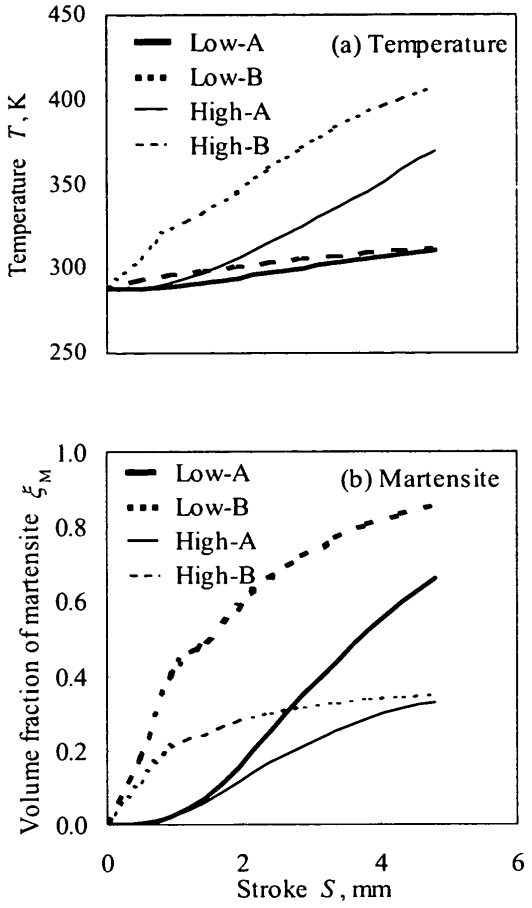

Fig. 6. Variation of temperature and volume fraction of martensite with progressive stroke at Point A and B of backward extrusion.

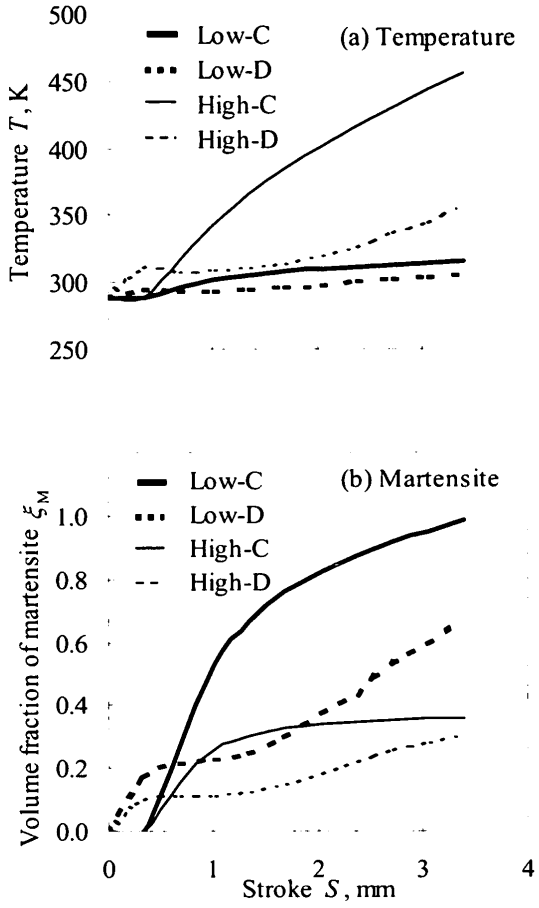

Fig. 7. Variation of temperature and volume fraction of martensite with progressive stroke at Point C and D of forward extrusion.

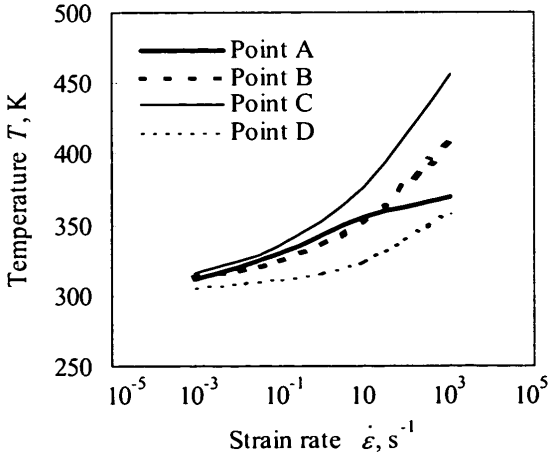

Fig. 8. Temperature versus strain rate.

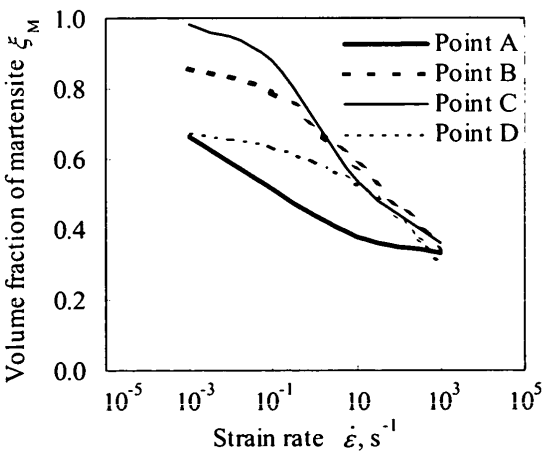

Fig. 9. Volume fraction of martensite versus strain rate.

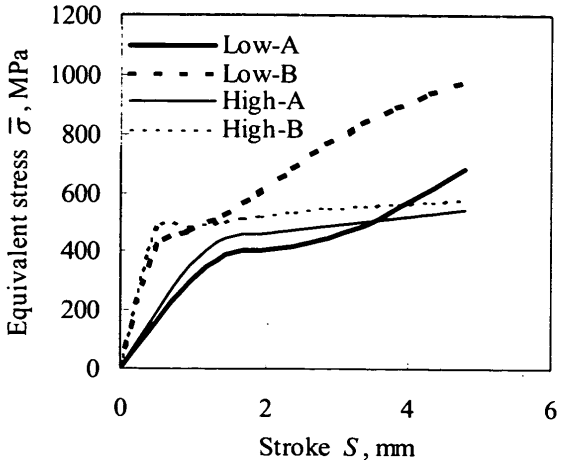

Fig. 10. Variation of equivalent stress with progressive stroke at Point A and B of backward extrusion.

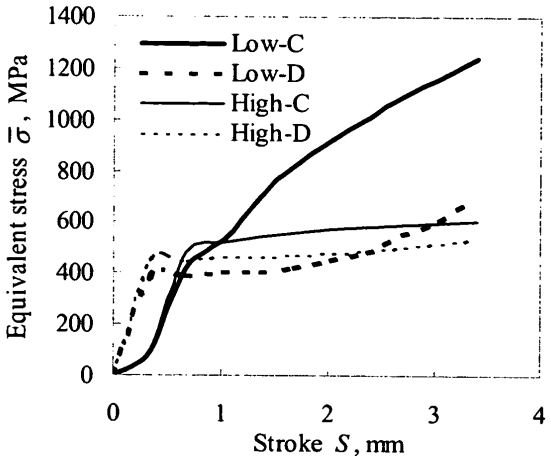

Fig. 11. Variation of equivalent stress with progressive stroke at Point C and D of forward extrusion.

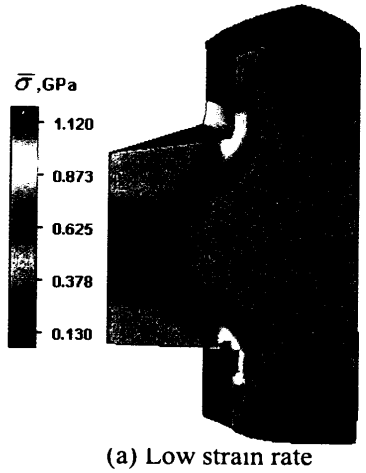

(a) Low strain rate

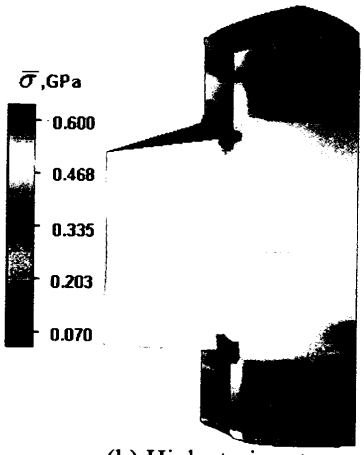

(b) High strain rate

Fig. 12. Calculated equivalent stress distributions after backward extrusion.

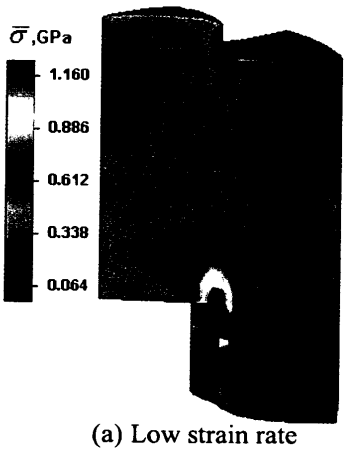

(a) Low strain rate

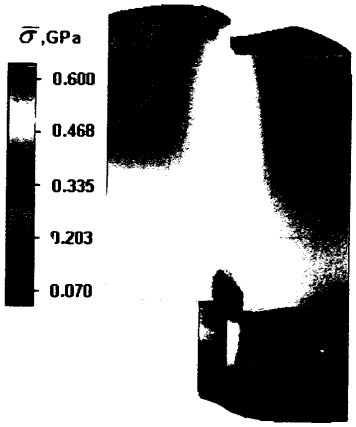

(b) High strain rate

Fig. 13. Calculated equivalent stress distributions after forward extrusion.

4. CONCLUSION

A finite volume method in the framework of Eulerian formulation is applied to simulate the forging process coupled with strain-induced phase transformation. To demonstrate the feasibility of this method a series of simulations on backward and forward extrusions have been used as examples. The simulation results on the volume fraction of martensite and forging load show a good agreement in tendency with the experimental ones.

The effect of strain rate is very important on structural change and mechanical behavior. High strain rate results in sufficient adiabatic heating to inhibit the transformation and thereby change the flow stress. As seen from the simulations, it is necessary to simulate the forging with structural change taken into account.

Numerical analysis is a good tool to obtain detailed information and let the designer control the forging process in advance to operation. The finite volume technique has a great advantage, compared with the finite element method, such that it is available for severe deformation modes where the numerical implementation by the finite element method sometimes falls in unsatisfactory results due to the unexpected distortion. From this point of view, the finite volume method is expected to be a powerful tool in simulating metal forming processes.

A real three-dimensional forging process (without axi-symmetric condition) will be published in a separate paper.

Acknowledgments – The authors gratefully express their appreciation to Professor T. Tsuta, Hiroshima University, Professor T. Ishikawa, Nagoya University, for their kind provision of experimental data.

REFERENCES

1. T. Inoue, S. Nagaki, T. Kishino and M. Monkawa, Ing. Arch., **50** (1981) 315.
2. T. Inoue, Thermal Stresses III, Elseiver Science Publishers B.V. (1989) 192-278.
3. G.W. Powell, Trans. ASM, **50** (1958) 479
4. T. Angel, J. Iron Steel Inst., **177** (1954) 165.
5. G.B. Olson and M. Cohen, Met. Trans. A, **6A** (1975), 791.
6. S.S. Hecker, M.G. Stout, K.P. Staudhammer and J.L. Smith, Met. Trans. A, **13A** (1982) 619.
7. L.E. Murr, K.P. Staudhammer and S.S. Hecker, Met. Trans., A, **13A** (1982) 627.
8. Y. Tomita and T. Iwamoto, Int. J. Mech. Sci., **37** (1995) 1292.
9. D.C. Ludwigson and J.A. Berger, J. Iron Steel Inst., **207** (1969) 63.
10. J. A. Cortes R., T. Tsuta, Y. Mitani and K. Osakada, JSME Int. J., **35** (1992) 201.
11. T. Tsuta and J. A. Cortes R., JSME Int. J., **36** (1993) 63.
12. N. Kawai, H. Saiki and H. Hirate, J. of the JSTP, **17** (1976) 899 (in Japanese).
13. K. Shinagawa, H. Nishikawa, T. Ishikawa and Y. Hosoi, Iron and Steel, **3** (1990) 156 (in Japanese).
14. J. A. Cortes R. and T. Tsuta, Memoirs of the Faculty of Engineering, Hiroshima University, **11** (1993) 35.
15. J.R. Low and F. Garofalo, Proc. Soc. Exper. Stress Analysis, (1947) 16.
16. M. Gensamer, Trans. ASM, **36** (1946) 30.
17. J.H. Holloman, Trans. AIME, **162** (1945) 268.
18. M. Miyao, Z.G. Wang and T. Inoue, J. Soc. Mat. Sci., **35** (1986) 1352 (in Japanese).
19. W.J. Slagter, C.J.L Florie and A.C.J. Venis, Proc. of the 15th National Conference on Manufacturing Research, (1999) 73.
20. P. Ding, D.Y. Ju, T. Inoue and E. de Vries, Acta Metall. Sin. (Eng. Lett.), **1** (2000) 270.
21. C. Hirth, Numerical Computation of Internal and External Flows, Volume 2: Computational Methods for Inviscid and Viscous Flows, John Wiley & Sons (1990).
22. D.Y. Ju, T. Inoue and H. Matsui, Advances in Engineering Plasticity and its Applications, Elsevier Science Publishers (1993) 521.
23. I. Ohnaka, Introduction of Heat Transfer and Solidification Analysis – Application on Casting Process, Maruzen Publisher (1985) (in Japanese).